Chemical Engineering Journal 434 (2022) 134652

Contents lists available at ScienceDirect

Chemical Engineering Journal

journal homepage: www.elsevier.com/locate/cej

Anti-Defect engineering toward high luminescent efficiency in whitlockite phosphors

Xin Pan [a,b], Lefu Mei [a,*], Yixi Zhuang [b,*], Takatoshi Seto [c], Yuhua Wang [c], Mikhail Plyaskin [d], Wei Xi [e], Chao Li [e], Qingfeng Guo [f], Libing Liao [a,*]

[a] Beijing Key Laboratory of Materials Utilization of Nonmetallic Minerals and Solid Wastes, National Laboratory of Mineral Materials, School of Materials Sciences and Technology, China University of Geosciences, Beijing 100083, PR China
[b] State Key Laboratory of Physical Chemistry of Solid Surface, Fujian Provincial Key Laboratory of Materials Genome and College of Materials, Xiamen University, Xiamen 361005, PR China
[c] Key Laboratory for Special Function Materials and Structural Design of the Ministry of Education, National & Local Joint Engineering Laboratory for Optical Conversion Materials and Technology, School of Physical Science and Technology, Lanzhou University, No. 222, South Tianshui Road, Lanzhou, Gansu 730000, PR China
[d] Department of Engineering Physics and Radioelectronic, Siberian Federal University, 79 Svobodny Ave, Krasnoyarsk 660041, Russia
[e] Center for Electron Microscopy, TUT-FEI Joint Laboratory, Tianjin Key Laboratory of Advanced Porous Functional Materials, Institute for New Energy Materials & LowCarbon Technologies, School of Materials Science and Engineering, Tianjin University of Technology, Tianjin 300384, PR China
[f] School of Gemology, China University of Geosciences, Beijing 100083, PR China

ARTICLE INFO

Keywords:
Phosphors
Quantum efficiency
Defect engineering
Positron annihilation technique
Density functional theory
LED

ABSTRACT

Lacking an effective strategy to simultaneously address the challenges of quantum efficiency, luminescence intensity and thermal stability has become the key bottleneck for further development and large-scale application of solid-state lighting technology. Herein, inspired by the defect-engineering used in photoelectrocatalytic and photovoltaic materials, we acted in a diametrically opposite way and unprecedentedly proposed an anti-defect engineering strategy to develop high-efficiency phosphors. By constructing a rigid structure and introducing alkali metals *M* to remove cation vacancy defects, similar to building blocks and jigsaw puzzle, we developed three groups of whitlockite phosphors, namely $Ca_{3-x}Sr_x(PO_4)_2$:Ce^{3+}, $Ca_3(PO_4)_2$:Ce^{3+},*M* and $(Ca_{0.5}Sr_{0.5})_3(PO_4)_2$:$Ce^{3+}$,$Na^+$,$Mn^{2+}$, and synchronously realized the significant enhancement of photoluminescence intensity (2.46 times), thermal stability (87.92% at 150 °C), cathodoluminescence intensity (3.34 times), quantum yield (from 38.90% to 99.07%). We characterized the defect concentration by positron annihilation technique (PAT), and calculated Debye temperature (*ΘD*) and simulated the occupation of *M* according to DFT theory to reveal the improvement mechanism. Some advanced applications were also explored in this work, including warm-white LEDs, plant growth lighting and information security. The anti-defect engineering proposed in this work may contribute to the further development of high-efficiency phosphors for the next-generation smart solid-state lighting technologies.

1. Introduction

Since humans lit the first torch, the quest for more efficient and environmentally friendly lighting sources has never stopped. The applications of various artificial lighting devices, including incandescent, halogen, xenon, fluorescent lamps, and white light-emitting diodes (WLEDs), allow us to illuminate the world in an ever more convenient and efficient way. Among them, phosphor-converted-WLEDs (pc-WLEDs) technology has become the dominant lighting type because of its high efficiency, environmental friendliness, long lifetime, and flexible applicability. However, there is still large room for the pc-WLED technology considering the needs of different application fields.[1] Phosphors are one of the most significant components in pc-WLEDs, which largely determine the performance of the lighting devices.[2] Nowadays, although there are many commercial phosphors such as oxides, sulfides, nitrides, fluorides, *etc*., unfortunately, there all have

Abbreviations: TCP:Ce, $Ca_3(PO_4)_2$:0.07Ce^{3+}; TCSP:Ce, $Ca_{3-x}Sr_x(PO_4)_2$:0.07Ce^{3+}; TCP:Ce,*M*, $Ca_3(PO_4)_2$:0.07Ce^{3+},0.07*M*; *M*, Li^+, Na^+, and K^+; TCSP:Ce,Na,Mn, $(Ca_{0.5}Sr_{0.5})_3(PO_4)_2$:0.07$Ce^{3+}$,0.07$Na^+$,y$Mn^{2+}$.

* Corresponding authors.
E-mail addresses: mlf@cugb.edu.cn (L. Mei), zhuangyixi@xmu.edu.cn (Y. Zhuang), clayl@cugb.edu.cn (L. Liao).

https://doi.org/10.1016/j.cej.2022.134652
Received 12 December 2021; Received in revised form 5 January 2022; Accepted 8 January 2022
Available online 14 January 2022

some short-board of performance, such as low color rendering of aluminates, high spectral reabsorption and manufacturing costs of nitrides, poor stability of silicates and fluorides.[3] In particular, phosphates have good stability but generally have low efficiency, and the same dilemma also exists widely in red phosphors with larger stokes-shift.

In the past few decades, material scientists and engineers spent great efforts to develop all kinds of phosphors with appropriate emission spectra, superior luminous intensity, high quantum yield (QY), and excellent chemical/thermal stability (TS).[4] Several methods, including experimental-oriented methods, artificial intelligence (AI) and machine learning[5], have been reported to explore new phosphors and regulate the luminescent performance[6,7], such as combined chemistry screening[8], genetic algorithm-assisted combinatorial search[9], single-particle diagnosis approach[10], high-throughput computing [11], mineral inspired prototype evolution[12], chemical unit cosubstitution[13], and new phase construction[14], *etc*. These design methods have extensively promoted the development of phosphors for WLEDs.[15,16] Still, the discovery of phosphors simultaneously showing several outstanding optical properties, especially those with both high QY and excellent stability, remains a significant challenge. [17–20]

Defects widely exist in actual phosphors. There has been evidence that zero-dimensional (0D) point defects such as oxygen vacancies may significantly affect the luminescence intensity and thermal quenching performance of phosphors.[21] They could be harmful to luminescence by direct annihilation of incident photons or complex energy transfer processes.[22] For example, Due to energy transfer from Eu^{3+} to vacancy defects and non-radiative transition, the QY of $ZnMoO_4$:Eu^{3+} dropped sharply from 70% to 32%, accompanied by a decrease of luminescence lifetime from 0.58 to 0.34 ms.[23] The same situation was also reported in $SrZnO_2$:Eu^{3+}[24], ZrO_2:Eu^{3+}[25], Mg_2SiO_4:Re^{3+} (Re = Eu, Tb)[26], *etc*. Alternatively, defects in some phosphors could contribute positively to the luminescence by giving new emission bands, abnormal thermal quenching, or delayed emission features (afterglow). [27] Several examples of a significant performance enhancement can be found in phosphors, photocatalytic materials, and photovoltaic materials.[28–30] Obviously, effective defect engineering, through accurately introducing or manipulating specific species of defects, should be an essential method to achieve required properties in luminescent materials.[31] Nevertheless, the understanding on the effects of specific defects on the optical performance in phosphors is limited.

In this work, we proposed anti-defect engineering methods in whitlockite phosphor families belonging to phosphate and accordingly constructed phosphors with a rigid structure and fewer vacancy defects that possessed greatly enhanced luminescence efficiency and promising applications (Fig. 1). On the one hand, Sr was introduced into the cation site of Ca. A solid solution system was formed to improve its crystallinity and structure rigidity. The more rigid structure reduced the energy loss

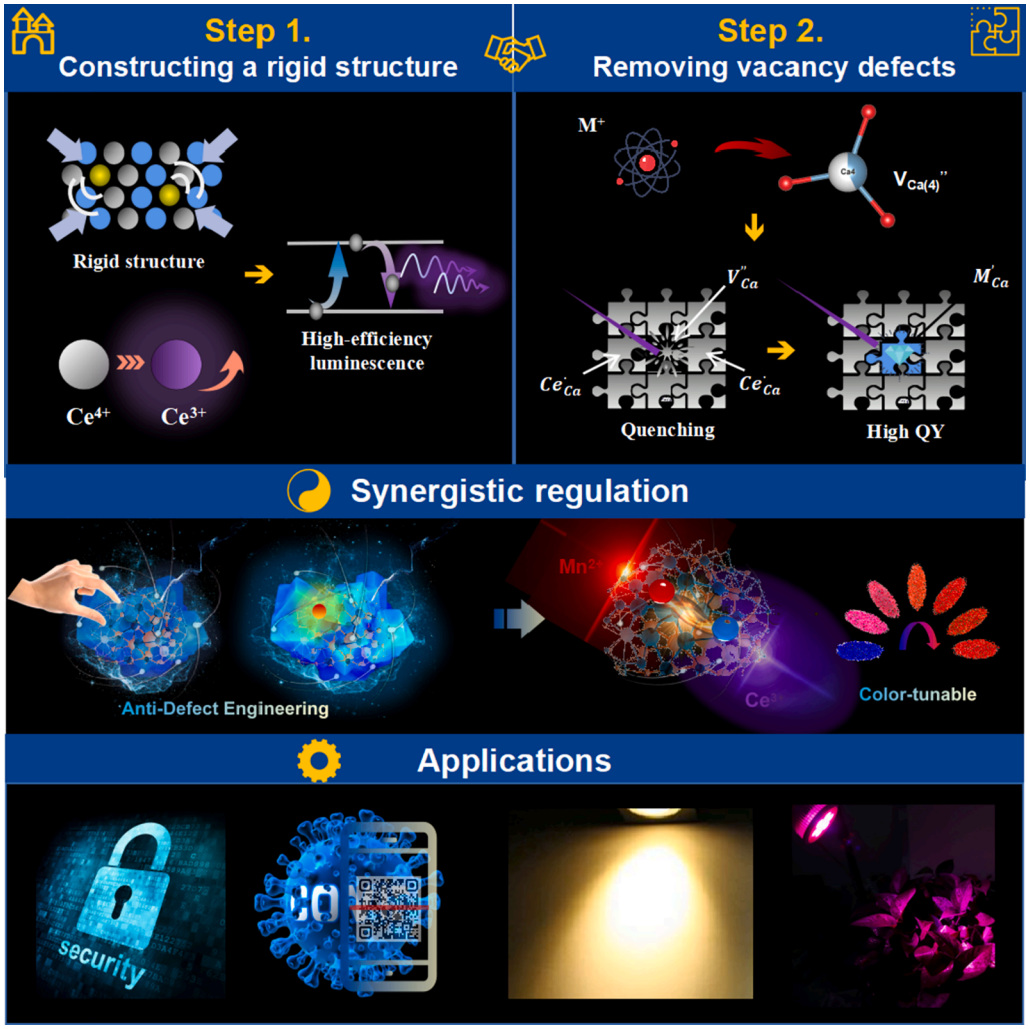

Fig. 1. Schematic diagram of composition design, property regulation, and potential applications of whitlockite phosphors in this research. The main property regulation methods include (i) constructing a rigid structure and (ii) eliminating vacancy defects, which are proven highly effective for improving luminescence efficiency.

and contributed to photon emission. On the other hand, alkali metal ions were introduced into the phosphors, which removed the cation vacancy defects as emission quenchers. This research has made efforts to achieve a number of comprehensive improvements in performance, and especially the quantum efficiency has increased from 38% to nearly 100%. We further combined the two strategies to develop a high-efficiency red phosphor by efficient energy transfer. Finally, we explored the potential applications in this work in the fields of warm-white LEDs, plant growth lighting, information security, and anti-counterfeiting.

2. Results and discussion

2.1. Constructing a rigid structure in solid-solution system

Phosphates are important hosts for high-efficiency phosphors. [32,33] Among them, tricalcium phosphates $Ca_3(PO_4)_2$ and their derivatives (well known as whitlockite in mineralogy) have attracted much attention due to the rich/adjustable crystallographic structure, suitable bandgap, good chemical stability, and excellent substitutability for some rare-earths.[34–42] Consequently, based on the optimal concentration obtained from our previous research, we started from the compound $Ca_3(PO_4)_2$:0.07Ce^{3+} (abbreviated as TCP:Ce) and replaced Ca^{2+} with Sr^{2+} to synthesize phosphors with compositions of $Ca_{3-x}Sr_x(PO_4)_2$:0.07Ce^{3+} [abbreviated as TCSP:Ce ($0 < x \leq 3$)].[43] The X-ray powder diffraction (XRPD) examinations indicated that the diffraction patterns of TCP:Ce and TCSP:Ce ($x = 0.5, 1, 1.5$) were well indexed to a rhombohedral structure with the space group of *R3c* [PDF #09–0169, $Ca_3(PO_4)_2$] (Fig. 2**a**). With the increase of Sr content x up to 1.5, the diffraction peaks gradually shifted towards the low-angle direction, and no impurity phase was observed, suggesting that a Ca-Sr-mixing solid solution was formed. In the compounds with Sr content of more than 1.5, however, new diffraction patterns attributed to another rhombohedral crystal with the space group of *R3m* appeared [PDF #24–1008, $Sr_3(PO_4)_2$]. Thus, when x was larger than 1.5, the phase transformation from *R3c* to *R3m* occurred in the TCSP:Ce system. [44,45]

The crystal structures generated from Rietveld analysis results of the *R3c* ($x = 0$) to *R3m* ($x = 3$) phases are presented in Fig. 2**b, Figure S1 and Table S1-S3 (Supporting Information)**. The *R3c* phase shows a more complex structure, with Ca^{2+} ions coordinated in five different polyhedrons [coordination number 7, 8, 8, 3, and 6 from Ca(1) to Ca(5), respectively] and P^{5+} ions in three different polyhedrons[46]. On the other hand, the *R3m* phase contains only two different Ca^{2+} polyhedrons and one [PO_4] group.[47] The centers of the polyhedrons can be replaced by other isovalent or aliovalent cations, making it possible to design new isostructural phases. ^{31}P solid-state magic-angle spin nuclear magnetic resonance (MAS-NMR) study was carried out to probe the variation of chemical environments around the P^{5+} ions. As depicted in Fig. 2**c**, multiple peaks were recorded in the TCP:Ce and TCSP:Ce ($x = 0.5, 1, 1.5$) samples. The multiple peaks gradually merged with the increase of Sr content and finally converted to a single peak when $x = 3$. The evolution of the ^{31}P chemical shift was well consistent with the phase transformation when the Sr content was larger than 1.5.

High-resolution transmission electron microscope (HRTEM) images and diffraction patterns (from three different directions, Fig. 3**a**) confirmed the single phase of solid solution in the TCSP:Ce ($x = 1.5$) phosphors. The grain with good dispersion and size between 1 ~ 5 μ m, which is conducive to the preparation of WLED and other related devices. Element mapping of the TCSP:Ce ($x = 1.5$) particles by scanning electronic microscopy (SEM) show uniform distribution of atoms in a reasonable proportion **(**Fig. 3**b)**. Meanwhile, in the HRTEM image of the TCSP:Ce ($x = 2$) sample, biphasic boundaries and different lattice stripes were observed, again indicating that phase transformation occurred (Fig. 3**c**).

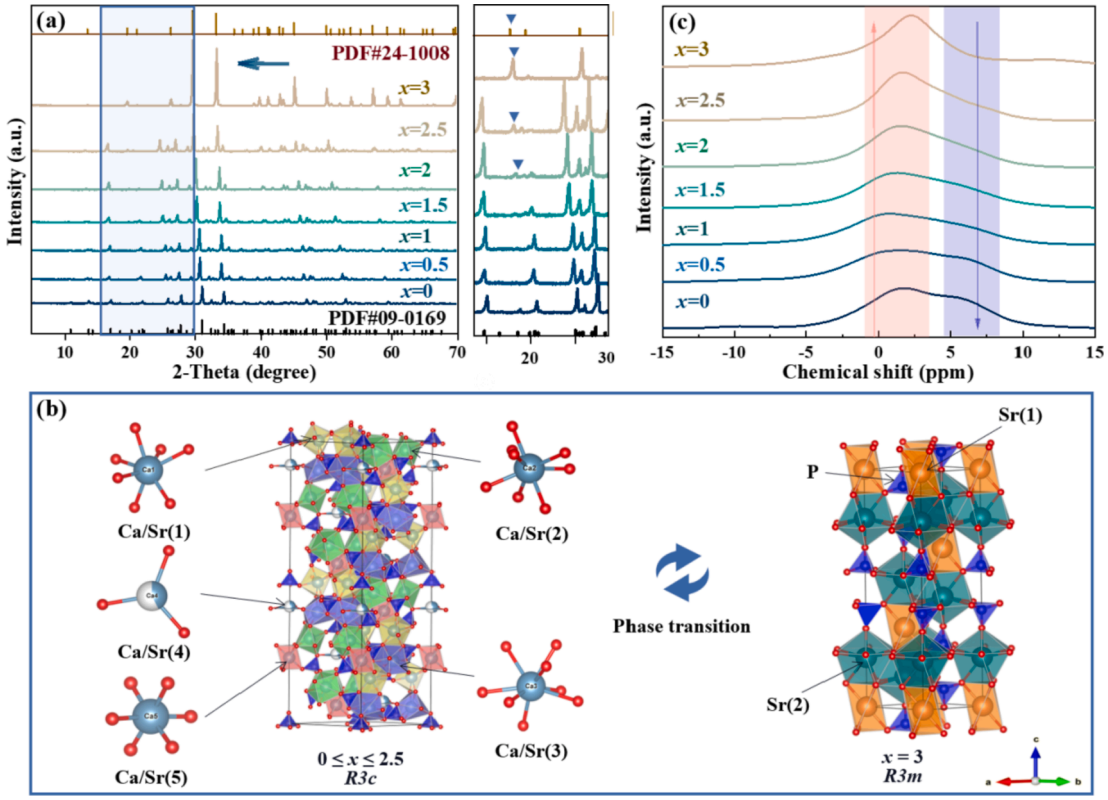

Fig. 2. (a) XRPD patterns of TCP:Ce and TCSP:Ce ($0 < x \leq 3$) with the standard PDF cards. (b) Crystal structures of $Ca_3(PO_4)_2$ (space group *R3c*) and $Sr_3(PO_4)_2$ (space group *R3m*). (c) ^{31}P MAS-NMR spectra of TCP:Ce and TCSP:Ce ($0 < x \leq 3$). Solid solutions of $Ca_{3-x}Sr_x(PO_4)_2$:Ce^{3+} were formed for x less than 1.5, and phase transformation occurred when x was larger than 1.5.

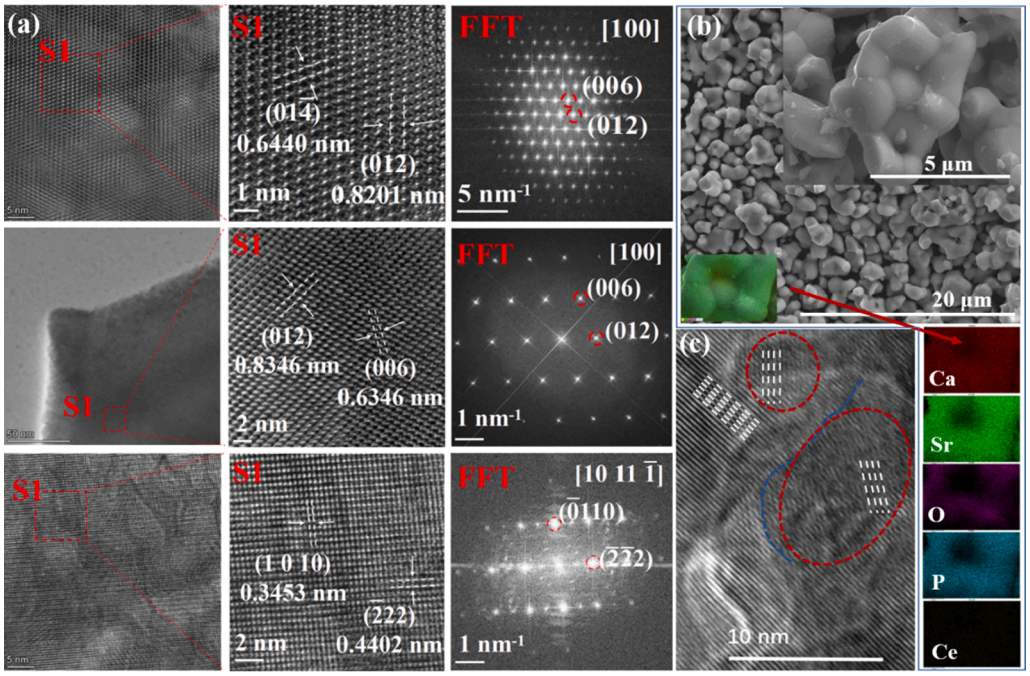

Fig. 3. (a) HRTEM images and diffraction patterns from three different directions of TCSP:Ce ($x = 1.5$). (b) Dispersion, grain image, and element mapping of O, Ca, Ce, P, and Sr by SEM in the TCSP:Ce ($x = 1.5$) phosphor. (c). HRTEM images of different lattice fringes, regions (red) and interfaces (blue) in biphasic system observed in TCSP:Ce ($x = 2$). (For interpretation of the references to color in this figure legend, the reader is referred to the web version of this article.)

After the structure and morphology of the phosphor, the main luminescence properties were further revealed. The characteristic broadband emissions of all the TCP:Ce and TCSP:Ce ($0 < x \leq 3$) phosphors at ~ 360 nm under ultraviolet excitation (Fig. 4**a)** illustrate the successful entry of Ce^{3+} into the cation position in the lattice. The excitation spectrum covered from 240 to 330 nm (**Figure S2, Supporting Information**). The broadband emissions were attributed to the Laporte's allowed electric dipole transitions of Ce^{3+}: 5d-4f with $^2F_{5/2}$ and $^2F_{7/2}$ transitions of Ce^{3+} fall back to the ground states respectively, which is merge reflected in the further broadening of the spectrum. Check the photoluminescence (PL) relative strength of the whole series for comparison under ensuring appropriate and fixed setting parameters. The PL intensity was enhanced when the Sr content increased, reaching 2.43 times of the initial intensity (TCP:Ce) at the optimal composition of TCSP:Ce ($x = 1.5$). The quantum efficiency measurements showed similar results. Under the same excitation at 310 nm, the internal quantum efficiency (IQE) increased from 38.90% (TCP:Ce) to 44.18% (TCSP:Ce, $x = 1$), 40.99% ($x = 1.5$) and then decreased to 38.81% ($x = 2$), 37.52% ($x = 2.5$), and 30.37% ($x = 3$) (Fig. 4**b)**.

Debye temperature (ΘD) model was used to represent the structural rigidity of the studied phosphors, which provides an estimate of the temperature at which all vibration modes of a crystal are activated.[48] Fewer phonon modes can be obtained in a rigid lattice with high ΘD at a given temperature, reflecting a lighter energy loss due to thermal vibration.[49] The values of ΘD were estimated by using DFT calculations, and they were plotted in Fig. 4**c** and **Table S4, Supporting Information**. The results showed that the ΘD value increased from 541 (TCP:Ce) to 730 K [TCSP:Ce ($x = 1.5$)] and declined with a further increase of Sr content. The increase of ΘD value in the range of $0 \leq x \leq 1.5$ was reasonable since more heavy atoms Sr entered the solid solution, thus constructing a more rigid structure. However, it should be noted that the structure rigidity could be broken with a further increase of Sr content (when x is larger than 1.5) due to the phase transformation. The Debye temperature model established a relationship between the luminescent efficiency and the structure of the studied $Ca_{3-x}Sr_x(PO_4)_2:Ce^{3+}$ solid solutions, indicating that a more rigid structure was favorable to achieve higher luminescent efficiency. Similar results have been reported in the studies of $Y_3Al_5O_{12}$:Ce[50], $Sr[LiAl_3N_4]:Eu^{2+}$[51], *etc.* A general explanation is that the probability of non-radiative transitions by lattice vibration should be reduced in a host with higher structure rigidity, thus contributing to higher luminescence efficiency (Fig. 4**e**) and better thermal quenching performance (**Figure S3, Supporting Information**).

Furthermore, high-resolution X-ray photoelectron spectroscopy (XPS) was measured to investigate the surface valence states of Ce ions in the phosphors, which were used as evidence of the overall valence of the reaction to a certain extent thanks to the good chemical stability of phosphors. The Ce^{3+} ratio (binding energies at 900.86 and 882.61 eV) to the total Ce ions (binding energies of Ce^{4+} at 896.99 and 878.41 eV) increased from 29% (TCP:Ce) to [TCSP:Ce ($x = 1.5$)] and then decreased (Fig. 4**d**). This indicated that more Ce^{3+} ions might be incorporated into the solid solutions, which also could contribute to the enhancement of luminescence efficiency. In addition, according to the Gibbs equation [52], the entropy (ΔS_e) increase induced by solid solution and biphasic can reduce the temperature barrier of the reaction and promote the improvement of crystallinity to a certain extent.

2.2. Removing vacancy defects via alkali metal codoping

Furthermore, we synthesized the second series of phosphors with compositions of $Ca_3(PO_4)_2$:0.07Ce^{3+},0.07 M ($M = Li^+$, Na^+, and K^+). These phosphors are named TCP:Ce,Li, TCP:Ce,Na, and TCP:Ce,K, respectively. The XRPD patterns showed that trace codoping of alkali metal did not change the crystalline phase with *R3c* space group (Fig. 5**a)**. The surface of TCP:Ce,Na particles was analyzed with a spherical aberration electron microscope (STEM) (Fig. 5**b)**. The high angle annular dark field image (HAADF) and annular bright-field image (ABF) images observed in the same direction indicated that the atoms were arranged orderly according to the crystal structure of $Ca_3(PO_4)_2$ (*R3c*). By analyzing the high-resolution transmission electron microscope (HRTEM) images and the diffraction patterns along three different orientations, we found that the spacing of the (0 1 2) crystal planes decreased from 0.8346 (TCP:Ce) to 0.7998 nm (TCP:Ce,Na), which verified the incorporation of alkali metal into the crystal lattice (Fig. 5**c)**. Also, XPS signals of alkali metals could be detected in the phosphors

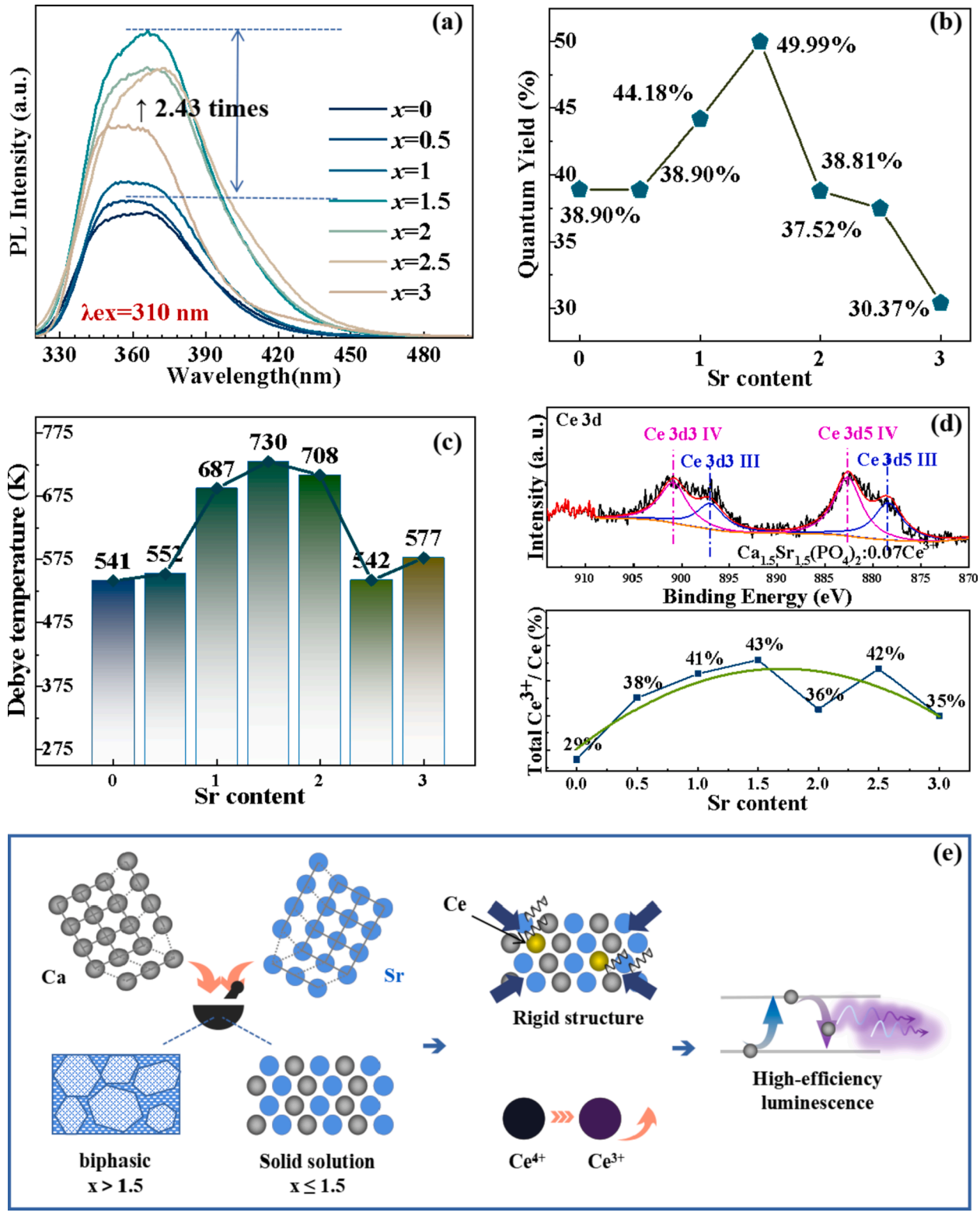

Fig. 4. (a) PL spectra of TCP:Ce and TCSP:Ce ($0 < x \leq 3$) under 310 nm excitation. (b) IQE under 310 nm excitation. (c) Debye temperature (ΘD) estimated with DFT calculations. (d) Top: high-resolution XPS energy spectra Ce in TCSP:Ce ($x = 1.5$) and bottom: ratio of Ce^{3+} in TCP:Ce and TCSP:Ce ($0 < x \leq 3$). (e) Schematic diagram of improving performance by forming Solid solution-biphasic system, increasing entropy and enhancing the rigid host-structure.

washed with water (Fig. 7**a**). Thus, the alkali metals should enter into the crystal lattice rather than be adhere to the surface as raw material.

The three alkali-metal-codoping phosphors showed broadband emission spectra centered at ~ 360 nm similar to TCP:Ce. Compared with the TCP:Ce phosphor, the PL intensity increased by 2.46, 1.61, and 1.24 times in the TCP:Ce,Li, TCP:Ce,Na and TCP:Ce,K, respectively (Fig. 6**a**). Meanwhile, the thermal quenching of emission was suppressed in the codoping phosphors. The PL intensity recorded at 150 °C in the TCP:Ce,Li TCP:Ce,Na and TCP:Ce,K kept 78.33%, 87.92% and 69.67% of the value at 25 °C, compared with 45.81% in the TCP:Ce (Fig. 6**b**). The

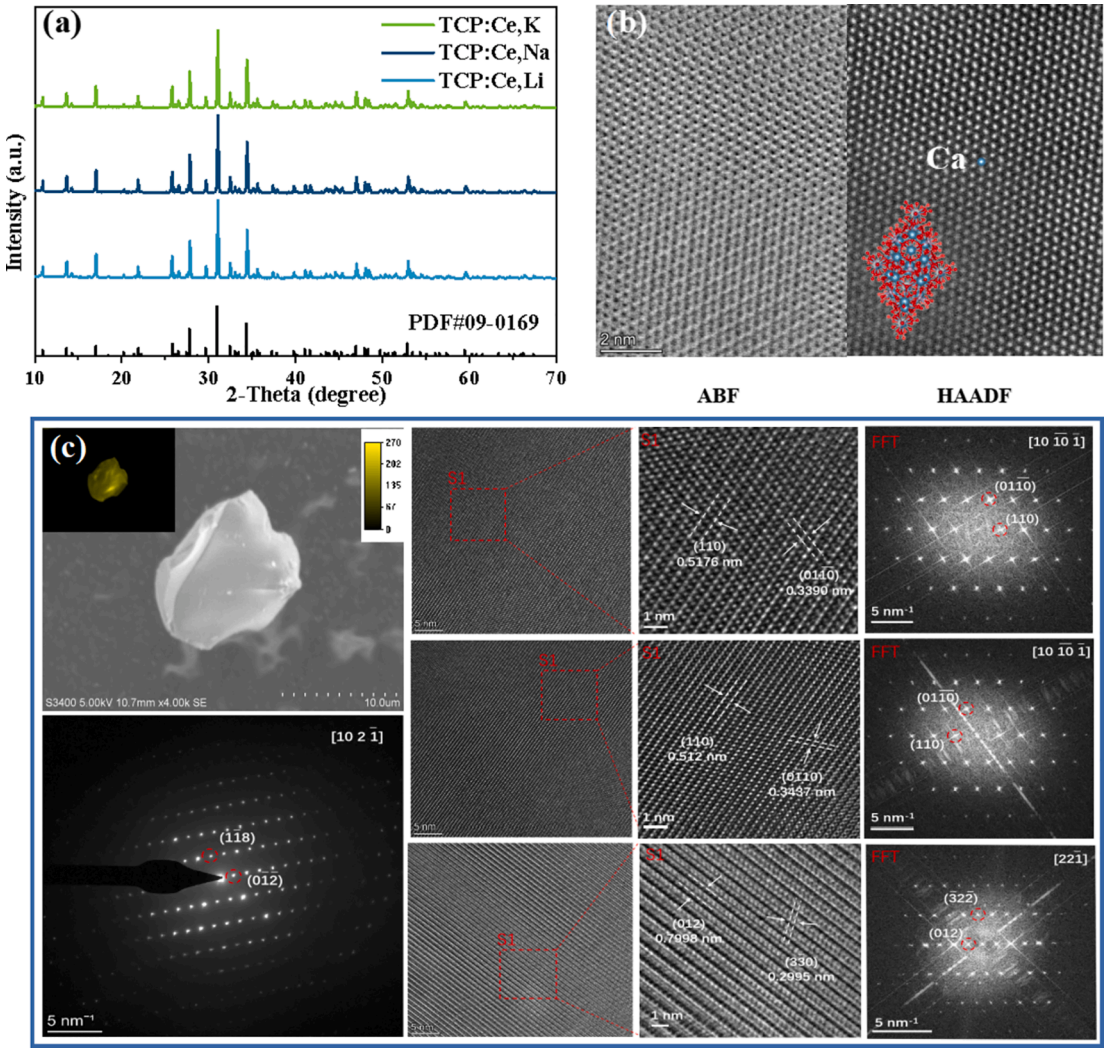

Fig. 5. (a) XRPD patterns of the TCP:Ce,Li, TCP:Ce,Na and TCP:Ce,K phosphors. The bottom gives the standard PDF card of $Ca_3(PO_4)_2$. (b) STEM-ABF and HAADF images of the surface structure of TCP:Ce,Na. (c) HRTEM images of TCP:Ce,Na and diffraction patterns along three different orientations.

cathodoluminescence (CL) of the TCP:Ce and TCP:Ce,Na phosphors were investigated with a field emission scanning electron microscope (FESEM). In both cases, the CL intensity grew up monotonously with the increases of applied current and accelerating voltage (**Fig. 6c and 6d**). [53] Under the same conditions, the maximum CL intensity of TCP:Ce, Na was 3.34 times higher than that of TCP:Ce. Excitingly, the IQE was significantly improved from 28.66% (TCP:Ce) to 96.05% (TCP:Ce,Li), 99.07% (TCP:Ce,Na), and 96.92% (TCP:Ce,K), accompanied by a high value of the external quantum yield (EQE) at 73.15% (TCP:Ce,Li), 77.33% (TCP:Ce,Na), and 74.26% (TCP:Ce,K), respectively (**Fig. 6e**). The greatly enhanced PL efficiency and thermal quenching performance are significant for solid-state lighting applications, especially for high-power lighting technology.

Previous studies have found that adding alkali metal ions into the lattice may improve the luminescence properties of some phosphors [54,55]. However, the detailed mechanism was complex, and it should depend on the specific phosphors. In this work, the possible reason for the significant improvement of luminescence efficiency and thermal quenching resistance is discussed from the viewpoint of the defect reaction equation.

During the solid-state reaction of $Ca_3(PO_4)_2$:Ce^{3+}, a part of Ce ions (from raw materials CeO_2) were incorporated into the host and reduced to Ce^{3+} states (probably to $Ce^{\bullet}_{Ca}$). Still, there existed charge unbalance in this substitution reaction. This resulted in the formation of negative point defects $V_{Ca}^{''}$ for charge conservation according to the following equation (Kröger-Vink notation, superscript ' for a negative charge, · for a positive charge, and × for a neutral state):

$$4CeO_2+4H_3PO_4 \xrightarrow{Ca_3(PO_4)_2} 4Ce^{\bullet}_{Ca}+2V_{Ca}^{''}+4P_P^{\times}+16O_O^{\times}+6H_2O\uparrow+O_2\uparrow \quad (1)$$

These vacancy defects $V_{Ca}^{''}$ were adjacent to the luminescent center $Ce^{\bullet}_{Ca}$ and could have a negative effect on luminescence [56,57]. Meanwhile, different from the effective luminescence center Ce^{3+}, the electronic configuration of Ce^{4+} is the same as that of inert atom Xe, with a full shell outer layer, which can not produce the front electron transition radiation., which could be quenchers for Ce^{3+} emission.[58]

When alkali metal (M) oxides were co-doped with CeO_2 into the $Ca_3(PO_4)_2$:Ce^{3+} phosphor (the same concentration of M and Ce), the defect reaction equation should be changed to:

$$2M_2O+4CeO_2+\frac{16}{3}H_3PO_4 \xrightarrow{Ca_3(PO_4)_2} 4Ce^{\bullet}_{Ca}+4M^{'}_{Ca}+\frac{16}{3}P_P^{\times}+\frac{64}{3}O_O^{\times}+8H_2O\uparrow+O_2\uparrow \quad (2)$$

A supercell $Ca_{21}P_{14}O_{56}$ was established, and the formation probability of $M^{'}_{Ca}$ was evaluated with DFT simulation by taking Li as an example. The simulation results indicated that among five different cationic crystallographic positions or lattice gaps $Li_i^{\cdot}$, the formation energy of $Li^{'}_{Ca}$ in the Ca(4) site was lowest (**Fig. 7b**, **Table S5**, **Supporting**

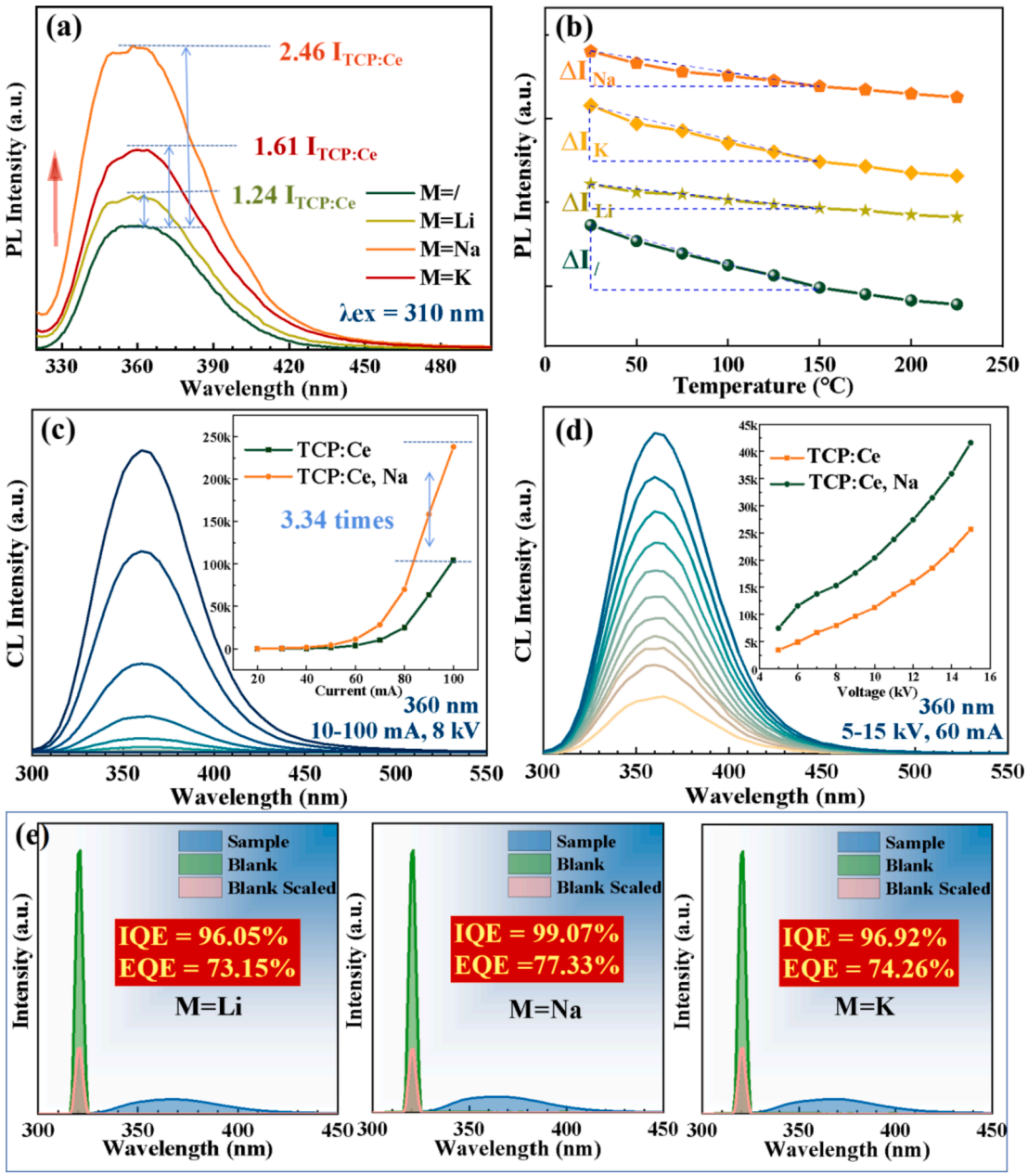

Fig. 6. (a) PL spectra of TCP:Ce, TCP:Ce,Li, TCP:Ce,Na and TCP:Ce,K under 310 nm excitation. (b) PL intensity as a function of temperature (from 25 to 225 °C) in four samples. (c) CL spectra of TCP:Ce,Na under 10–100 mA and 8 kV. The inset shows the CL intensity of TCP:Ce and TCP:Ce,Na as a function of applied current. (d) CL spectra of TCP:Ce,Na under 60 mA and 5–15 kV. The inset shows the CL intensity of TCP:Ce and TCP:Ce,Na as a function of accelerating voltage. (e) IQE of TCP:Ce,Li, TCP:Ce,Na and TCP:Ce,K.

Information). Since that the alkali metal M should also occupy the Ca^{2+} sites, the numbers of vacancy defects $V_{Ca}^{''}$ should be decreased and replaced by $M_{Ca}^{\cdot}$. We performed positron annihilation lifetime spectra on the TCP:Ce, TCP:Ce,Li, TCP:Ce,Na, and TCP:Ce,K samples. The results supported that the level of vacancy defects was pulled down after codoping of alkali metals (Fig. 7**c**). Also, XPS measurements on the Ce valence states indicated that the Ce^{3+} ratios in the phosphors with alkali metals were increased on a large scale (from 28.66% for TCP:Ce to 57.91%, 57.26%, and 55.09% for TCP:Ce,Li, TCP:Ce,Na, and TCP:Ce,K, see Fig. 7**d**, Fig. 7**e, and Table S6, Supporting Information**). This may be attributed to the fact that the addition of alkali metals promoted the defect reaction in **Eq.** (1)**,** making more Ce^{3+} enter the Sr^{2+} sites, which was also simply described as the charge compensation effect in the studies of other phosphor.[55] At the same time, the alkali metal oxide could also work as a flux during the solid-state reaction and promote the reduction of Ce ions.

In this section, like an interesting jigsaw puzzle, we found that codoping three kinds of alkali metals greatly enhanced the luminescence efficiency and thermal quenching performance of $Ca_3(PO_4)_2:Ce^{3+}$, which could be majorly attributed to removing the vacancy defects $V_{Ca}^{''}$ and lifting the Ce^{3+} ratios. Among the three species of alkali metals, the TCP:Ce,Na phosphor presented the best performance. This was possible because the Na^{+} ions showed the closest radius with Ca^{2+} ions, which is in favor of the reaction of **Eq.** (2).

2.3. Synergistic regulation of luminescent efficiency for next-generation lighting technologies

The next-generation lighting technologies require phosphors with higher luminescence efficiency, appropriate spectral region and better

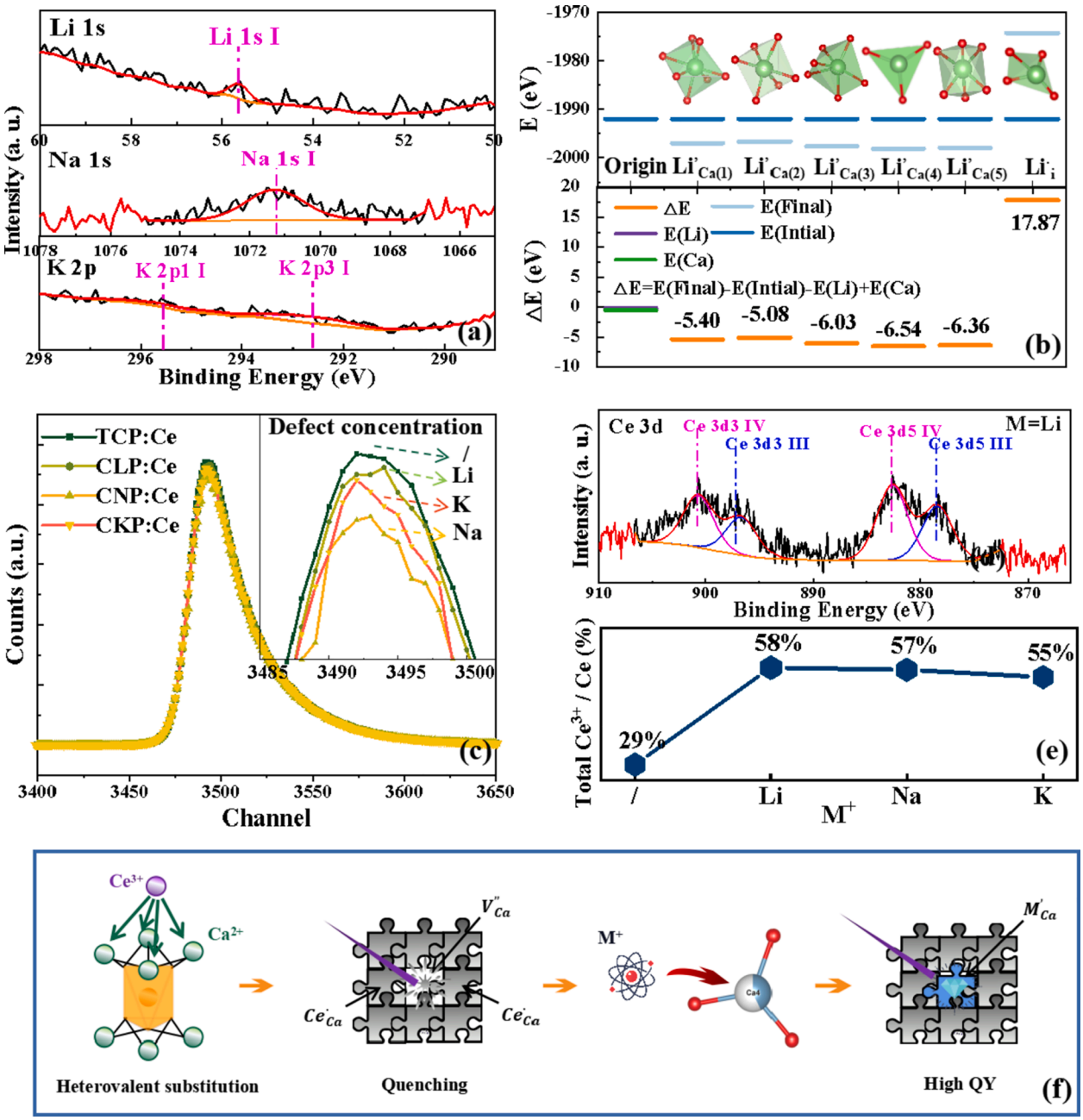

Fig. 7. (a) XPS spectra monitoring the valence states of Li, Na, and K. (b) The formation energies Δ E of five different cationic lattice sites and interstitial vacancies occupied by Li in the crystal were calculated by DFT theory. (c) Positron annihilation lifetime spectra to determine the defect concentrations. (d) XPS energy spectra. (e) The ratio of Ce^{3+} ions to the total Ce ions in TCP:Ce, CLP:Ce, CNP:Ce, and CKP:Ce according to the XPS results. (f) The schematic diagram for the improvement of luminescence by removing vacancy defects.

luminescence stability. Importantly, higher luminescence efficiency can greatly reduce the energy consumption of lighting devices. Based on the results of Sections 2.1 and 2.2, we combined with strategies of cation substitution and self-charge compensation, and accordingly developed a new red phosphor namely $(Ca_{0.5}Sr_{0.5})_3(PO_4)_2$:0.07$Ce^{3+}$,0.07$Na^{+}$,y$Mn^{2+}$ ($0 \leq y \leq 0.11$, abbreviated as TCSP:Ce,Na,Mn). Notably, the codoping of Mn^{2+} as emitters enabled the improvement of luminescent efficiency to be extended to the red region, which is important for the applications in warm-white LEDs and plant growth lighting.

The synthesized TCSP:Ce,Na,Mn phosphors exhibited structural stability up to 1000 °C and excellent resistance to humility, acid and base solutions (**Figure S4**, **Supporting Information**). The TCSP:Ce,Na,Mn phosphors showed an intense emission band centered at 620 nm and weak emission at around 360 nm upon excited with UV light (**Figure S5**, **Supporting Information**). The red emission was majorly attributed to the Mn^{2+}:$^4T_1 \rightarrow {}^6A_1$ electronic transition *via* an energy transfer process from Ce^{3+} to Mn^{2+}.

We further fabricated two LED lamps by using the TCSP:Ce,Na,Mn phosphors to demonstrate potential applications initially. The related devices are manually packaged and manufactured by single component TCSP:Ce,Na,Mn or adding commercial phosphor, 310 nm UV-LED chip, gold wire, support and UV curing active material (Fig. 8**a**). The monitored device spectra, CIE coordinates and photographs of two lamps as shown in Fig. 8**b and** Fig. 8**c**. The device performance parameters (CIE coordinates, CCT, and Ra) are shown in **Table S7**, **Supporting Information**. In the first lamp, the TCSP:Ce,Na,Mn phosphors were packaged as a red-LED lamp, and the emission spectra were mainly located in the red region from 580 to 760 nm. Early studies have stated that only about

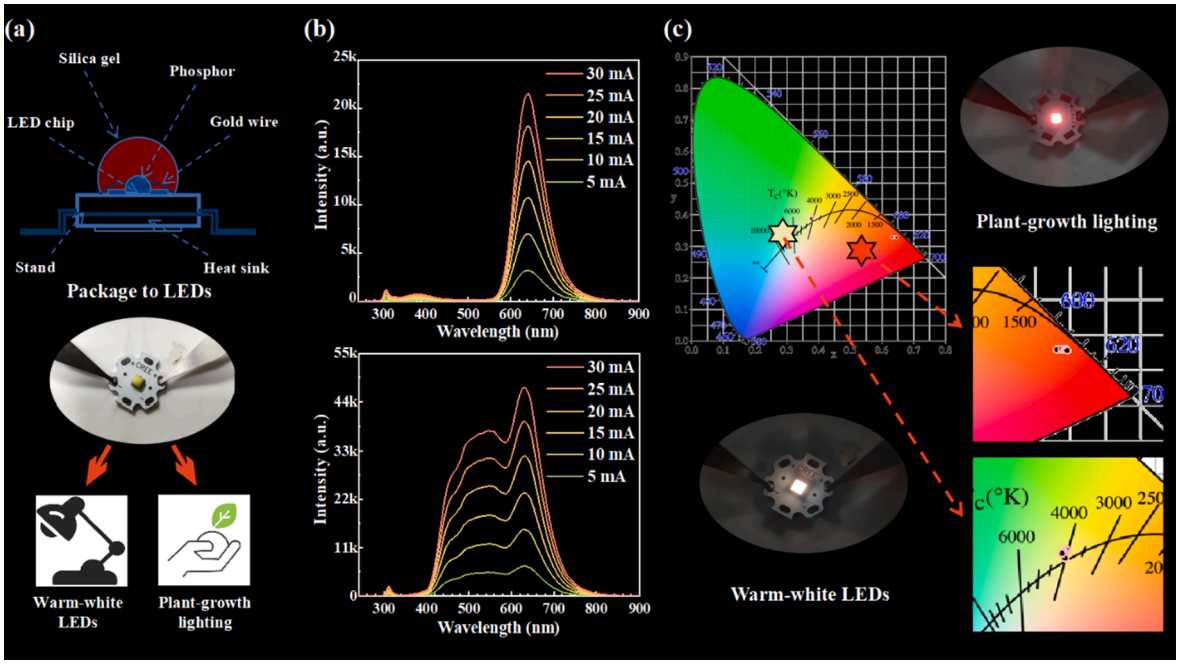

Fig. 8. (a) Packaging the developed phosphors to LED lamps. (b) The monitored device spectra at different currents (5–30 mA) single component TCSP:Ce,Na,Mn (up) and combination of mixed commercial phosphors (down). (c) The CIE coordinates and photographs of two lamps for warm-white LED (left) and plant-growth lighting (right).

5% of the solar radiation spectrum affects photosynthesis. The blue light (400–500 nm) can promote the growth of stem and leaf; red light (600–750 nm) can regulate the flowering cycle, which can accelerate the development of plants significantly, cause the plants to bloom, and set up early, which plays a leading role in plant color enhancement.[59] Besides, near-infrared light (850–1100 nm) can regulate root growth and nutrient absorption. The emission spectra of the red-LED lamp matched well with the requirement of absorption spectra for most green plants. The correlated color temperature (CCT) $\leq$ 2800, color rendering index (Ra) $\geq$ 35, high colour purity value recline in the region from 89.21 to 92.67 and excellent color stability, and thus it was suitable for the application in plant growth lighting. In the future modern agricultural development models, we can further design the time (or cycle), intensity, and spectrum (or light quality) of the plant growth lamp according to plant growth needs to control the illumination accurately to improve the yield and quality of plants.

In the second lamp, the TCSP:Ce,Na,Mn phosphors were combined with BAM ($BaMgAl_{10}O_{17}:Eu^{2+}$), YAG ($Y_3Al_5O_{12}$: Ce^{3+}, Ga^{3+}). The emission spectra covered the whole visible region from 400 to 750 nm. The CIE coordinate is located in the warm white region with CCT $\leq$ 4150 and Ra $\geq$ 89. It has been a fact that if the CCT has a value less than 5000 K, it is appropriate for the warm red light for the solid-state lighting applications. Also, the fabricated LED lamp showed excellent color stability upon long-term working. The above results indicated the TCSP: Ce,Na,Mn phosphor could be a good candidate of red phosphor component for the application in warm-white LEDs. To some extent, our initial attempt showed the potential to solve the problem that it is difficult to obtain low CCT with a single YAG: Ce^{3+} phosphor (low CCT standard: less than 4500 K), but there are still challenges to match with mass production chips to be further overcome.[60,61] Based on its good chemical and thermal stability, we consider that if the phosphor is mixed in ink and printed into an information security code or anti-counterfeiting pattern, it can also play a positive role in security protection. In any case, the anti defect engineering strategy may provide a new idea in the performance improvement of phosphors and the relationship between performance and crystal defects, also show the expected application potential in a variety of LED phosphors.

3. Conclusion

An anti-defect engineering strategy was proposed in this work to develop high-efficiency phosphors for energy-saving applications. By constructing a rigid structure and removing vacancy defects $V_{Ca}^{''}$, which was similar to building blocks and jigsaw puzzles, significant improvement of PL intensity (2.46 times), thermal stability (87.92% at 150 °C), CL intensity (3.34 times), IQE (sharply improved from 38.9% to 99.07%), and EQE (up to 76.89%) was achieved. The potential mechanism has been excavated - by forming a solid solution system to improve its crystallinity and structural rigidity, the more rigid structure reduces the energy loss caused by lattice vibration and improves the radiation transition of photons; via introducing alkali metal ions, the cation vacancy defect as emission quencher is eliminated, and the light energy conversion efficiency is significantly improved. Several advanced applications were explored, including warm-white LEDs, plant growth lighting, or anti-counterfeiting patterns for information security. In a nutshell, this novel design inspiration could be a promising strategy to comprehensively improve the luminescence performance, quantum efficiency, luminescence intensity and thermal stability of phosphors. Meanwhile, the angle of establishing the relationship between properties and crystal defects, and the potential applications mined, may open up a brand-new path for creating more phosphors or related products with luminous characteristics that meet the needs of the contemporary era.

4. Experimental Section/Methods

4.1. Material and synthesis

Although sol–gel, hydrothermal, spray pyrolysis, and combustion methods have been reported to synthesize phosphors, considering the simplest and suitable for mass, the solid-state reaction method at high-temperature production was selected, and two groups of Ce^{3+} doped phosphors $Ca_{3-x}Sr_x(PO_4)_2$:0.07$Ce^{3+}$and $Ca_3(PO_4)_2$: 0.07Ce^{3+},0.07 *M* (*M* = Li^+, Na^+ and K^+), as well as one group of Ce^{3+} and Mn^{2+} codoped phosphors $(Ca_{0.5}Sr_{0.5})_3Na_{0.07}(PO_4)_2$:0.07$Ce^{3+}$,y$Mn^{2+}$ were prepared by

it. Briefly, the starting materials $CaCO_3$, $SrCO_3$, $(NH_4)_2HPO_4$, CeO_2, Li_2CO_3, Na_2CO_3, K_2CO_3 and MnO_2 (99.99%, Aladdin company) were weighed according to the stoichiometry, and the amount of all cation sites has subtracted the overall doping concentration of Ce^{3+}, M^+ and Mn^{2+}. Then thoroughly ground by hand in an agate mortar for 30 min and placed the mixture in a corundum crucible, and preheated at 850 °C for 1 h to release NH_3, H_2O, and CO_2 in a muffle furnace in the air. Finally, under the reducing atmosphere of 10% H_2 − 90% N_2, the samples were ground and sintered again for 10 h in a tubular furnace at 1250 °C. After slowly cooling to room temperature, the product was ground into fine powder and repeatedly washed with pure deionized water for three times to remove impurities for subsequent characterization.

4.2. Measurements and characterization

The powder diffraction data of phosphors for Rietveld analysis were collected at room temperature with a Bruker D8 ADVANCE powder diffractometer (Cu-Kα radiation) and linear VANTEC detector. The step size of 2θ was 0.02°, and the counting time was 2 s per step. High-temperature in-situ X-ray diffraction adopts 0–1600 °C table heating, heating range 25 °C to 1000 °C, vacuum 10^{-3}, heating rate 50 °C per minute. The morphologies of samples were characterized by field emission scanning electron microscopy (FE-SEM, EOL, JSM-7900F, Japan) at 20 kV. The microscope was equipped with energy-dispersive X-ray spectroscopy (EDS, Oxford, X-MAX) by Jem-2100 plus microscope (Joel, Japan). More detailed structural imaging characterization, such as High-resolution transmission electron microscope (HRTEM) images, electron diffraction patterns and atomic structure images, were collected by special error corrected transmission electron microscope (AC-TEM) of Tianjin University of technology. The types of images collected are HADDF and ABF (Joel). The X-ray photoelectron spectroscopy (XPS) measurement was done on a Thermo Scientific Escalab Xi spectrometer using 150 W Al Kα X-ray sources, and all the binding energies were referenced to the C1s peak at 284.6 eV of the surface adventitious carbon.

Photoluminescence (PL) and photoluminescence excitation (PLE) spectra were detected by a FLUOROMAX-4P photoluminescence spectrophotometer (Horiba Jobin Yvon, New Jersey, U.S.A.), equipped with a 150 W xenon lamp, and the step length was set up to be 1.0 nm. Thermal stability was tested using a heating apparatus (TAP-02) in combination with PL equipment. The absolute quantum yield (IQE) was examined by Hamamatsu photonic multi-channel analyzer C10027. The quantum yield was calculated using the data measured by FLS 920 fluorescence spectrometer of integrating sphere (Edinburgh Instruments, UK) at room temperature. The cathodoluminescence (CL) performance was tested on the modified Mp-Micro-S instrument attached to the SEM. The four-component lifetimes of TCP:Ce and TCP:Ce,*M* were measured by positron annihilation lifetime spectroscopy (PALS) to characterize their defect concentrations. By simultaneously measuring two BaF_2 scintillation detectors and using the time difference between the rise of the two waveforms.

The VASP package was employed to perform the structural geometry relaxation of the host matrices. Structural models were adopted from ICSD data. The generalized gradient approximation and automatically generated 4 × 4 × 4 k points were employed in the calculations. The energy cut-off of the plane-wave basis was set to 520 eV. The convergence criterion for the electronic energy was 10^{-5} eV, and the structures were relaxed until the Hellmann-Feynman forces were less than −0.02 eV/Å. The Debye temperature (*ΘD*) was also estimated using density functional theory (DFT) calculations with the generalized gradient approximation (GGA-PBE) exchange–correlation functional to describe the interactions. An increased plane wave cut-off energy of 520 eV was used for cell optimization. The electronic iteration convergence was 10^{-5} eV using the normal (blocked Davidson) algorithm and reciprocal space projection operators. An explicit k-mesh of 4 × 4 × 4 was employed.

4.3. Application devices

WLED: the blue powder BAM ($BaMgAl_{10}O_{17}$: Eu^{2+}) and the yellow-green powder $Y_3Al_5O_{12}$: Ce^{3+}, Ga^{3+} were mixed with TSCP:Ce, Na,0.09Mn the ratio of 3:1:2; SLED: only TCSP:Ce,Na,0.09Mn phosphor. UV curing adhesive was used, the mass ratio of powder to adhesive was 1:1, the LED chip was 0.2 W, 310 nm.

Declaration of Competing Interest

The authors declare that they have no known competing financial interests or personal relationships that could have appeared to influence the work reported in this paper.

Acknowledgments

This work was financially supported by the National Natural Science Foundation of China (41802040). The authors would like to acknowledge Prof. Zhendong Hao from Changchun Institute Optics-Fine Mechanics and Physics, Chinese Academy of Sciences, Prof. Rong-Jun Xie, Dr. Shuxing Li and Dr. Cunjian Lin from Xiamen University, Prof. Xin Min and Prof. Zhijian Peng from China University of Geosciences (Beijing), Dr. Haikun Liu from Dongguan University of Technology, and Dr. Chenglong Zhao from Institute of Physics, Chinese Academy of Sciences for their kind suggestions to the manuscript. The authors also thank Dr. Zebin Li and Mrs. Cancan Li from Lanzhou University for their help on the experiments.

Appendix A. Supplementary data

Supplementary data to this article can be found online at https://doi.org/10.1016/j.cej.2022.134652.

References

[1] P. Pust, P.J. Schmidt, W. Schnick, A revolution in lighting, Nature Materials 14 (5) (2015) 454–458.
[2] W.-Y. Huang, F. Yoshimura, K. Ueda, Y. Shimomura, H.-S. Sheu, T.-S. Chan, H. F. Greer, W. Zhou, S.-F. Hu, R.-S. Liu, J.P. Attfield, Nanosegregation and neighbor-cation control of photoluminescence in carbidonitridosilicate phosphors, Angewandte Chemie-International Edition 52 (31) (2013) 8102–8106.
[3] K.M. Kim, J.H. Ryu, Synthesis of $Y_3Al_5O_{12}$:Ce^{3+} colloidal nanocrystals by pulsed laser ablation and their luminescent properties, Journal of Alloys and Compounds 576 (2013) 195–200.
[4] Z. Xia, Q. Liu, Progress in discovery and structural design of color conversion phosphors for LEDs, Progress in Materials Science 84 (2016) 59–117.
[5] P. Raccuglia, K.C. Elbert, P.D.F. Adler, C. Falk, M.B. Wenny, A. Mollo, M. Zeller, S. A. Friedler, J. Schrier, A.J. Norquist, Machine-learning-assisted materials discovery using failed experiments, Nature 533 (7601) (2016) 73–76.
[6] Y.i. Wei, H. Yang, Z. Gao, Y. Liu, G. Xing, P. Dang, A.A.A. Kheraif, G. Li, J. Lin, R.-S. Liu, Strategies for designing antithermal quenching red phosphors, Advanced Science 7 (8) (2020) 1903060.
[7] G.J. Hoerder, M. Seibald, D. Baumann, T. Schröder, S. Peschke, P.C. Schmid, T. Tyborski, P. Pust, I. Stoll, M. Bergler, Sr[$Li_2Al_2O_2N_2$]:Eu^{2+}—A high performance red phosphor to brighten the future, Nature communications 10 (1) (2019) 1824.
[8] K.-S. Sohn, I.W. Zeon, H. Chang, S.K. Lee, H.D. Park, Combinatorial search for new red phosphors of high efficiency at VUV excitation based on the YRO_4 (R = As, Nb, P, V) system, Chemistry of Materials 14 (5) (2002) 2140–2148.
[9] Y.S. Jung, C. Kulshreshtha, J.S. Kim, N. Shin, K.-S. Sohn, Genetic algorithm-assisted combinatorial search for new blue phosphors in a (Ca, Sr, Ba, Mg, Eu)xByPzO system, Chemistry of Materials 19 (22) (2007) 5309–5318.
[10] N. Hirosaki, T. Takeda, S. Funahashi, R.-J. Xie, Discovery of new nitridosilicate phosphors for solid state lighting by the single-particle-diagnosis approach, Chemistry of Materials 26 (14) (2014) 4280–4288.
[11] S.J. Henderson, J.A. Armstrong, A.L. Hector, M.T. Weller, High-throughput methods to optically functional oxide and oxide–nitride materials, Journal of Materials Chemistry 15 (15) (2005) 1528–1536.
[12] X. Zhou, J. Qiao, Z. Xia, Learning from mineral structures toward new luminescence materials for light-emitting diode applications, Chemistry of Materials 33 (4) (2021) 1083–1098.
[13] Z. Xia, C. Ma, M.S. Molokeev, Q. Liu, K. Rickert, K.R. Poeppelmeier, Chemical unit cosubstitution and tuning of photoluminescence in the $Ca_2Al_{1-x}Mg_xAl_{1-x}Si_{1+x}O_7$:$Eu^{2+}$ phosphor, Journal of The American Chemical Society 137 (39) (2015) 12494–12497.

[14] Z. Wang, J. Ha, Y.H. Kim, W.B. Im, J. McKittrick, S.P. Ong, Mining unexplored chemistries for phosphors for high-color-quality white-light-emitting diodes, Joule 2 (5) (2018) 914–926.

[15] G. Li, Y. Tian, Y. Zhao, J. Lin, Recent progress in luminescence tuning of Ce^{3+} and Eu^{2+}-activated phosphors for pc-WLEDs, Chemical Society Reviews 44 (23) (2015) 8688–8713.

[16] Z. Xia, M.S. Molokeev, W.B. Im, S. Unithrattil, Q. Liu, Crystal structure and photoluminescence evolution of $La_5Si_{2+x}B_{1-x}O_{13-x}N_x:Ce^{3+}$ solid solution phosphors, Journal of Physical Chemistry C 119 (17) (2015) 9488–9495.

[17] Y.i. Wei, H. Yang, Z. Gao, Y. Liu, G. Xing, P. Dang, A.A.A. Kheraif, G. Li, J. Lin, R.-S. Liu, Strategies for designing antithermal-quenching red phosphors, Advanced Science 7 (8) (2020) 1903060.

[18] R.-J. Xie, N. Hirosaki, T. Suehiro, F.F. Xu, M. Mitomo, A simple, efficient synthetic route to $Sr_2Si_5N_8:Eu^{2+}$-based redphosphors for white light-emitting diodes, Chemistry of Materials 18 (23) (2006) 5578–5583.

[19] Z. Ma, Z. Shi, D. Yang, Y. Li, F. Zhang, L. Wang, X.u. Chen, D.i. Wu, Y. Tian, Y. u. Zhang, L. Zhang, X. Li, C. Shan, High color-rendering index and stable white light-emitting diodes by assembling two broadband emissive self-trapped excitons, Advanced Materials 33 (2) (2021) 2001367.

[20] Y. Chen, Y.e. Li, J. Wang, M. Wu, C. Wang, Color-tunable phosphor of Eu^{2+} and Mn^{2+} codoped $Ca_2Sr(PO_4)_2$ for UV light-emitting diodes, Journal of Physical Chemistry C 118 (23) (2014) 12494–12499.

[21] M.D. Bhatt, J.S. Lee, Recent theoretical progress in the development of photoanode materials for solar water splitting photoelectrochemical cells, Journal of Materials Chemistry A 3 (20) (2015) 10632–10659.

[22] S. Zhu, D. Wang, Photocatalysis: basic principles, diverse forms of implementations and emerging scientific opportunities, Advanced Energy Materials 7 (23) (2017) 1700841.

[23] L. Wang, S. Liu, X. Feng, C. Zhang, L. Zhu, J. Zhai, Y. Qin, Z.L. Wang, Flexoelectronics of centrosymmetric semiconductors, Nature Nanotechnology 15 (8) (2020) 661–667.

[24] X. Yu, X. Xu, C. Zhou, J. Tang, X. Peng, S. Yang, Synthesis and luminescent properties of $SrZnO_2:Eu^{3+}$, $^{M}+$ (M=Li, Na, K) phosphor, Materials Research Bulletin 41 (8) (2006) 1578–1583.

[25] D. Prakashbabu, H.B. Ramalingam, R. Hari Krishna, B.M. Nagabhushana, R. Chandramohan, C. Shivakumara, J. Thirumalai, T. Thomas, Charge compensation assisted enhancement of photoluminescence in combustion derived Li^+ codoped cubic $ZrO_2:Eu^{3+}$ nanophosphors, Physical Chemistry Chemical Physics 18 (42) (2016) 29447–29457.

[26] R. Naik, S.C. Prashantha, H. Nagabhushana, Charge compensation assisted enhancement of photoluminescence in combustion derived Li^+ codoped cubic $ZrO_2:Eu^{3+}$ nanophosphors, Optical Materials 72 (2017) 295–304.

[27] M. Martini, F. Meinardi, Thermally stimulated luminescence: new perspectives in the study of defects in solids, Rivista Del Nuovo Cimento 20 (8) (1997) 1–71.

[28] X. Duan, M. Yuan, K. Ou, W. Zhao, T. Tian, W. Duan, X. Zhang, L. Yi, Controlled preparation of undoped Zn_2GeO_4 microcrystal and the luminescent properties resulted from the inner defects, Materials Today Communications 27 (2021), 102359.

[29] Y. Cao, X. Wang, Z. Zhang, Y. Wang, Unraveling the defect-related luminescence in a Eu^{2+}-doped chlorosilicate phosphor, Journal of Physical Chemistry Letters 12 (2) (2021) 958–965.

[30] J. Liang, C. Li, Y. Cui, Z. Li, J. Wang, Y. Wang, Rational design of efficient orange-red to red thermally activated delayed fluorescence emitters for OLEDs with external quantum efficiency of up to 26.0% and reduced efficiency roll-off, Journal of Materials Chemistry C 8 (5) (2020) 1614–1622.

[31] Z. Luo, Y. Ouyang, H. Zhang, M. Xiao, J. Ge, Z. Jiang, J. Wang, D. Tang, X. Cao, C. Liu, W. Xing, Chemically activating MoS_2 via spontaneous atomic palladium interfacial doping towards efficient hydrogen evolution, Nature communications 9 (1) (2018) 2120.

[32] M. Zhang, J. Wang, W. Ding, Q. Zhang, Q. Su, Luminescence properties of $M_2MgSi_2O7:Eu^{2+}$ (M=Ca, Sr) phosphors and their effects on yellow and blue LEDs for solid-state lighting, Optical Materials 30 (4) (2007) 571–578.

[33] W.B. Im, N. George, J. Kurzman, S. Brinkley, A. Mikhailovsky, J. Hu, B.F. Chmelka, S.P. DenBaars, R. Seshadri, Efficient and color-tunable oxyfluoride solid solution phosphors for solid-state white lighting, Advanced Materials 23 (20) (2011) 2300–2305.

[34] Z. Xia, H. Liu, X. Li, C. Liu, Identification of the crystallographic sites of Eu^{2+} in $Ca_9NaMg(PO_4)_7$: structure and luminescence properties study, Dalton Transactions 42 (47) (2013) 16588.

[35] J. Qiao, J. Zhao, Z. Xia, A review on the Eu^{2+} doped β-$Ca_3(PO_4)_2$-type phosphors and the sites occupancy for photoluminescence tuning, Optical Materials: X 1 (2019), 100019.

[36] H. Ji, Z. Huang, Z. Xia, M.S. Molokeev, V.V. Atuchin, M. Fang, Y. Liu, Discovery of new solid solution phosphors via cation substitution-dependent phase transition in $M_3(PO_4)_2:Eu^{2+}$(M = Ca/Sr/Ba) quasi-binary sets, Journal of Physical Chemistry C 119 (4) (2015) 2038–2045.

[37] C.-H. Huang, Y.-C. Chiu, Y.-T. Yeh, T.-M. Chen, Novel Eu^{2+}-activated yellow-emitting $Sr_8MgLu(PO_4)_7$ phosphors for white-light near-ultraviolet LEDs, Materials Express 2 (4) (2012) 303–310.

[38] L. Jiang, R. Pang, D. Li, W. Sun, Y. Jia, H. Li, J. Fu, C. Li, S. Zhang, Tri-chromatic white-light emission from a single-phase $Ca_9Sc(PO_4)_7:Eu^{2+}$, $T^{b3}+$, $^{Mn}2+$ phosphor for LED applications, Dalton Transactions 44 (39) (2015) 17241–17250.

[39] B.I. Lazoryak, Comment on "Tuning of photoluminescence and local structures of substituted cations in xSr2Ca(PO4)2–(1–x)Ca10Li(PO4)7:Eu2+ phosphors", Chemistry of Materials 29 (8) (2017) 3800–3802.

[40] J. Qiao, Z. Zhang, J. Zhao, Z. Xia, Tuning of the compositions and multiple activator sites toward single-phased white emission in $(Ca_{9-x}Sr_x)MgK(PO_4)_7:Eu^{2+}$ phosphors for solid-sate lighting, Inorganic Chemistry 58 (8) (2019) 5006–5012.

[41] J. Zhang, Z. Hua, S. Wen, Luminescence of emission-tunable $Ca_{10}Li(PO_4)_7:Eu^{2+}$, Sr^{2+}, Mn^{2+} phosphors with various Eu^{2+} centers for LED applications, Journal of Alloys and Compounds 637 (2015) 70–76.

[42] Y. Li, H. Yu, D. Deng, Y. Hua, S. Zhao, G. Jia, H. Wang, L. Huang, Y. Li, C. Li, S. Xu, Color point tuning by partial Ba^{2+}substitution of Ca^{2+} in $(Ca_{1-x}Ba_x)_3(PO_4)_2$ phosphor for white light emitting diodes, Journal of Solid State Chemistry 199 (2013) 248–252.

[43] Y. Yuan, H. Lin, J.a. Cao, Q. Guo, F. Xu, L. Liao, L. Mei, A novel blue-purple Ce^{3+} doped whitlockite phosphor: Synthesis, crystal structure, and photoluminescence properties, Journal of Rare Earths 39(6) (2021) 621-626.

[44] S. Turkdogan, F. Fan, C.-Z. Ning, Color-temperature tuning and control of trichromatic white light emission from a multisegment ZnCdSSe heterostructure nanosheet, Advanced Functional Materials 26 (46) (2016) 8521–8526.

[45] H. Zhang, D. Yuan, X. Mi, X. Zhang, Z. Bai, X. Liu, J. Lin, Crystal structure and luminescence properties of $Na_2MMg(PO_4)_2:Eu^{2+}$ (M = Ca/Sr/Ba) phosphors, Journal of Alloys and Compounds 798 (2019) 119–128.

[46] M. Yashima, Y. Kawaike, Crystal structure and site preference of ba-doped α-tricalcium phosphate $(Ca_{1-x}Ba_x)_3(PO_4)_2$ through high-resolution synchrotron powder diffraction (x= 0.05 to 0.15), Chemistry of Materials 19 (16) (2007) 3973–3979.

[47] M. Yashima, A. Sakai, T. Kamiyama, A. Hoshikawa, Crystal structure analysis of β-tricalcium phosphate $Ca_3(PO_4)_2$ by neutron powder diffraction, Journal of Solid State Chemistry 175 (2) (2003) 272–277.

[48] N.C. George, A.J. Pell, G. Dantelle, K. Page, A. Llobet, M. Balasubramanian, G. Pintacuda, B.F. Chmelka, R. Seshadri, Local environments of dilute activator ions in the solid-state lighting phosphor $Y_{3-x}Ce_xAl_5O_{12}$, Chemistry of Materials 25 (20) (2013) 3979–3995.

[49] K.A. Denault, J. Brgoch, S.D. Kloß, M.W. Gaultois, J. Siewenie, K. Page, R. Seshadri, Average and Local Structure, Debye Temperature, and Structural Rigidity in Some Oxide Compounds Related to Phosphor Hosts, Acs Applied Materials & Interfaces 7 (13) (2015) 7264–7272.

[50] J. Brgoch, S.P. DenBaars, R. Seshadri, Proxies from ab initio calculations for screening efficient Ce^{3+} phosphor hosts, Journal of Physical Chemistry C 117 (35) (2013) 17955–17959.

[51] W. Volker, P. Philipp, H. Cora, Narrow-band red-emitting $Sr[LiAl_3N_4]:Eu^{2+}$ as a next-generation LED-phosphor material, Nature Materials 13 (2014) 891–896.

[52] D. Yu, Z. Xue, T. Mu, Eutectics: formation, properties, and applications, Chemical Society Reviews 50 (15) (2021) 8596–8638.

[53] H. Chen, Y. Wang, Photoluminescence and cathodoluminescence properties of novel rare-earth free narrow-band bright green-emitting $ZnB_2O_4:Mn^{2+}$ phosphor for LEDs and FEDs, Chemical Engineering Journal 361 (2019) 314–321.

[54] S. Liu, Y. Liang, H. Li, W. Zhang, D. Tu, Y. Chen, Color tuning of β-$Ca_3(PO_4)_2$-type phosphor with enhanced quantum efficiency via self-charge compensation for healthy and warm solid state lighting application, Chemical Engineering Journal 390 (2020), 124463.

[55] Y. Chen, Q. Guo, L. Liao, M. He, T. Zhou, L. Mei, M. Runowski, B. Ma, Preparation, crystal structure and luminescence properties of a novel single-phase red emitting phosphor $CaSr_2(PO_4)_2:Sm^{3+}$, $L^{i}+$, RSC Advances 9 (9) (2019) 4834–4842.

[56] C. Ge, J. Sun, Q. Tong, W. Zou, L. Li, L. Dong, Synergistic effects of CeO_2/Cu_2O on CO catalytic oxidation: Electronic interaction and oxygen defect, Journal of Rare Earths DOI (2021), https://doi.org/10.1016/j.jre.2021.08.014.

[57] R. Kırkgeçit, H. Özlü Torun, F. Kılıç Dokan, E. Öztürk, Optical and electrical conductivity properties of rare earth elements (Sm, Y, La, Er) co-doped Ce_O2, Journal of Rare Earths (2021), https://doi.org/10.1016/j.jre.2021.10.001.

[58] I. Ahmad, M.S. Akhtar, M.F. Manzoor, M. Wajid, M. Noman, E. Ahmed, M. Ahmad, W.Q. Khan, A.M. Rana, Synthesis of yttrium and cerium doped ZnO nanoparticles as highly inexpensive and stable photocatalysts for hydrogen evolution, Journal of Rare Earths 39 (4) (2021) 440–445.

[59] G.D. Massa, H.-H. Kim, R.M. Wheeler, C.A. Mitchell, Plant Productivity in Response to LED Lighting, Hortscience 43 (7) (2008) 1951–1956.

[60] R.-J. Xie, N. Hirosaki, Silicon-based oxynitride and nitride phosphors for white LEDs—A review, Science and Technology of Advanced Materials 8 (7-8) (2007) 588–600.

[61] H. Zhu, C.C. Lin, W. Luo, S. Shu, Z. Liu, Y. Liu, J. Kong, E. Ma, Y. Cao, R.S. Liu, X. Chen, Highly efficient non-rare-earth red emitting phosphor for warm white light-emitting diodes, Nature communications 5 (2014) 4312.